# Evaluation of Organ Dose following Radiotherapy of the Brain using Bio-Based Head Phantom Made From Soy-Lignin bonded *Rhizophora* spp.

Siti Hajar Zuber,<sup>a,\*</sup> Nurul Ab. Aziz Hashikin,<sup>b</sup> Nor Hafizah Ishak,<sup>c</sup> Nursyatina Abdul Raof,<sup>c</sup> Mohd Fahmi Mohd Yusof,<sup>d</sup> and Mohd Zahri Abdul Aziz <sup>c</sup>

The purpose of this work was to create and assess a bio-based head phantom made from bio-based resources for external beam radiotherapy dose planning and delivery in brain cancer. The custom-made head phantom was fabricated using Rhizophora spp. bonded with soy flour and lignin, and its potential as phantom material was evaluated in previous studies. Organs at risk and planning target volume were identified using the treatment planning system, which was guided by computed tomography raw images. Thermoluminescent dosimeters were placed into specific holes positioned throughout the head phantom following individual calibration. Head phantom was imaged, planned and irradiated by linear accelerator. The planned predicted doses by treatment planning system at the targeted volume and the organ at risk regions were obtained and compared with the dosimeter doses. The result revealed that the planning target volume and organ at risks were within the dose range calculated by the treatment planning system, except for lens, optic chiasm and brainstem. Verification of the treatment plans was implemented, and good agreement between measured values and those predicted by the treatment planning system was found. The custom-made, bio-based phantom's preliminary results have proved to be a valuable tool for the treatment dose verification, demonstrating its prospective as potential phantom material for use in radiotherapy.

DOI: 10.15376/biores.20.3.5694-5708

Keywords: Rhizophora spp.; Bio-based phantom; Thermoluminescent dosimeter; Absorbed dose; Treatment planning system

Contact information: a: Faculty of Health Sciences, Universiti Kebangsaan Malaysia, 50300, Kuala Lumpur, Malaysia; b: School of Physics, Universiti Sains Malaysia, 11800, Penang, Malaysia; c: Pusat Perubatan USM, Universiti Sains Malaysia, 13200, Penang, Malaysia; d: Faculty of Health and Life Sciences, Management & Science University, 40150 Shah Alam, Selangor, Malaysia; \*Corresponding author: hajarzuber@ukm.edu.my

#### INTRODUCTION

One of the most frequent intracranial tumours in adult patients is brain cancer metastases (Armocida *et al.* 2023) from any cancer, such as small cell carcinoma. If left untreated, brain metastasis has a terrible prognosis, with a median lifespan of less than two months (Gupta *et al.* 2009). Radiation therapy aims to mitigate the adverse impact of intracranial metastasis on survival and improve the health-related quality of life (Arora and Cascella 2021). Whole brain irradiation (WBRT) is frequently used to treat patients with brain metastases, particularly in palliative care, in order to achieve good control of gross tumour deposits, enhance the quality of life and lengthen survival (Park *et al.* 2019). The

recommended scheme for the radiotherapy treatment of WBRT includes a total dose of 30 Gy in ten daily fractions (Gibbs and Soltys 2008).

Previous literature reported that WBRT came to the forefront and became a standard of care for brain metastases following several ground-breaking publications by previous researchers (Vlachos *et al.* 2023). In the preceding article, it was claimed that 24 of the 38 patients who received doses of 30 to 40 Gy reported symptomatic relief, with about half of them living for little more than three months. Due to its extensive reach, ease of administration and relatively low cost, WBRT has also emerged as one of the primary therapies for patients with brain metastases. According to earlier research, WBRT offers patients with brain metastases excellent palliation, with a high percentage of patients reporting relief from symptoms like headache, reduced motor function and poor mentation by the end of the second week.

Characterising a phantom is a critical step in developing a model that accurately simulates the human body, particularly in terms of its radiation attenuation and interaction properties. To ensure its suitability for radiation studies, it is essential to thoroughly analyse the material's characteristics. Rhizophora has garnered considerable interest as a potential phantom material due to its remarkable similarity to soft tissue, making it a promising candidate for use in radiation dosimetry. *Rhizophora* spp., a type of mangrove tree, thrives abundantly in the muddy tidal plains commonly found along Malaysia's coastal areas. While global mangrove distribution has fluctuated throughout geological history, Malaysia ranks third among the top 20 nations with significant mangrove coverage, making Rhizophora spp. readily available (Hamilton and Casey 2016). Traditionally, Rhizophora spp. has been utilised for charcoal production, fuelwood, and as raw material for chipboard, pulpwood, and synthetic industries. Previous studies have highlighted the potential of Rhizophora-based phantom materials, emphasising their advantageous physical and mechanical properties, effective atomic number, attenuation characteristics and dosimetric properties (Samson et al. 2020; Samson et al. 2020; Samson et al. 2023; Zuber et al. 2023; binti Zuber et al. 2024).

Although dose measurement within the actual human body is not possible, phantom studies are widely used in the field of medical physics and radiotherapy (Yadav et al. 2023) to simulate the dose estimation received by the patient. The need to verify treatment planning using an anthropomorphic phantom is critical in WBRT (Gupta et al. 2009). Depending on the outcomes of the verification with phantom, the treatment planning accuracy was estimated and the plan was either approved or denied. The paradigm of anthropomorphic phantom in verifying treatment planning provides the best alternative in determining the dose delivery to the target area and importantly, to the organ at risk (OAR). Based on ICRU 50 (1993), OAR is defined as normal tissues and its radiation sensitivity may significantly influence treatment planning or prescribed dose (Monti et al. 1995; Chavaudra and Bridier 2001). In WBRT, OAR includes right and left lens, right and left eyeballs, parotid glands, right and left optic nerves and spinal cord. One of the best methods for accurate dose delivery and superiority check is in vivo dosimetry and for many years, thermoluminescent dosimeter (TLD) was the only option for any practical in vivo dose measurement although it began to be replaced by diodes in the recent years.

The TLD is a point dosimeter (Cederhag *et al.* 2023) that specialises in dosimetry in the low and high energy ranges. It is frequently used in radiotherapy and diagnostic research. It is necessary to have a thorough understanding of TLD behaviour in order to measure the dose with accuracy. In an experimental setting, it is possible to measure organ and surface dose by placing TLD in a specially designed anthropomorphic phantom. TLD

is a type of radiation dosimeter that is available in a variety of forms, from powder to circular chips, rods, cubes and in a range of materials (Tootell *et al.* 2014). TLDs are suitable for point dose measurement in high gradient regions due to their small size and allow for multiple points to be measured simultaneously (Radaideh 2017). Previous literature reported that photon beam radiotherapy requires dose calculation algorithms as well as practical in-vivo dosimetry audits for effective patient treatment (VanDam and Marinello 1994; Wesolowska *et al.* 2017). TLD has the benefit of being very sensitive even for a small irradiated volume, making it a particularly effective approach for in-vivo measurements.

Often employed in radiotherapy, the treatment planning system (TPS) generates beam shapes and dose distributions intending to maximise the dose to the tumour and minimise exposure of unneeded radiation to normal tissue. Inaccuracy owing to dosimetric errors between planned and delivered treatments from the simulation process through treatment execution is still a possibility, despite its primary function of properly determining the dose delivery to the target area. Significant discrepancies between estimated doses using TPS and actual doses from in-vivo dosimetry, particularly in the critical structures, were described in prior work (Chung *et al.* 2005). Thus, it would be valuable to investigate the calculation accuracy of the absorbed dose within the target area and OAR for clinically relevant radiotherapy treatment plans.

In this study, a bio-based head phantom made from bio-based soy-lignin bonded *Rhizophora* spp. was fabricated with TLD holes mimicking RANDO phantom to measure absorbed dose to target organs and OARs in the external beam radiotherapy technique for WBRT by using TLD and comparison was made with the dose estimation by TPS. While many previous studies have explored phantom development, they often lack clinical relevance due to simplified geometries such as water phantom or limited integration with TPS-based dose verification. This study addresses those gaps by introducing several novel features which are the use of soy-lignin bonded *Rhizophora* spp. as a sustainable and mechanically stable material, anatomical customisation to emulate the RANDO phantom, including TLD positioning, and direct dosimetric comparison under clinically relevant WBRT settings.

#### MATERIAL AND METHODS

# Fabrication of Head Phantom made from Soy-Lignin Bonded *Rhizophora* spp.

In this study, *Rhizophora* spp. wood trunks from Kuala Sepetang were used as raw material. For adhesive, commercially available soy flour and lignin in powder form were purchased from Sigma (Sigma Aldrich; Merck, QRec, Malaysia). Soy flour and lignin used were in powder form with no addition of hardener. The preparation for the fabrication of particleboard was explained in detail in the previous study (Zuber *et al.* 2020a). Particleboard fabricated from *Rhizophora* soy-lignin-bonded slabs was used to create the head phantom. The particleboard slabs were made by hot pressing at approximately 200 °C, with a pressure of 20 MPa for approximately 20 min. The soy flour and lignin as adhesives were used to solidify the bond between the wood particles. Slabs with a measurement of approximately  $(24.0 \times 24.0 \times 1.0)$  cm<sup>3</sup> were prepared at  $1.0 \text{ g} \cdot \text{cm}^{-3}$  target density. A commercially available RANDO phantom was used as a reference to construct the head phantom. Due to the thickness of the RANDO phantom (2.5 cm), which differs

from the fabricated particleboard (1.0 cm), a prototype was made using polystyrene. The polystyrene was cut into the required shape, and each polystyrene slab was then cut using a polystyrene cutter onto 1.0 cm slab thickness. Due to the non-uniform shape of the head, the particleboard was trimmed using a band saw and was sanded onto the required design. For the dosimetry study, small holes were made on the particleboard slabs before they were coated with a gloss finish. Extensive evaluation and characterisation of the soy-lignin bonded particleboard were carried out prior to this work (Zuber *et al.* 2022a, 2022b, 2021, 2020a, 2020b), and results revealed its potential as phantom material in radiation and dosimetry study.

## Computed Tomography (CT) Scanning of the Head Phantom for Treatment Planning

In a supine position, the specially designed head phantom was immobilised using support foam and sponge. The TLD slots were drilled in accordance with a specified specification. Due to post-drilling of the phantom in certain area, the TLD representing right parotid, left parotid, right optic nerve and left optic nerve were estimated during the TPS point dose measurement. Two fiducial markers were placed on both sides of the head, one fiducial marker was placed at the anterior point of the head, and the laser was set at the centre with a constant couch position. CT images were acquired using head routine protocol (RTP Head and Neck HCT 3 mm) with an exposure factor of 120 kVp using the CT scanners (Toshiba Aquilion) at Advanced Medical and Dental Institute, Universiti Sains Malaysia. CT images were acquired from vertex to level of C7 at 3 mm slice thickness with the implementation of adaptive iterative dose reduction three-dimensional (AIDR 3D) with and without the TLD placement in each slab.

## TPS Monaco for Organ Delineation and Planning

Clarification and three-dimensional delineation of the target area and organ at risk are the first phases in the radiotherapy planning procedure. The head phantom CT simulation's raw CT data was exported into TPS Monaco for further planning and delineation. The CT Digital Imaging and Communications in Medicine (DICOM) images were accrued and transferred to the TPS Monaco. Monaco may provide a set of functions that allow the calculation and measurement of the penalty when transgressing an individual or objective restriction used for the optimisation of the treatment plan (Rodriguez 2018). Biological optimisation is very beneficial in terms of conformity and homogeneity (Rodriguez 2018). Monaco may also use restriction parameters in optimisation.

In TPS, the 3D shape of a contour is derived from a set of 2D contours drawn on the CT image. TPS Monaco was used to plan the 6 MV direct anterior beam (field size: 10 × 10 cm²) on the head phantom. Before the delineation of the target area in TPS, DICOM data was transferred to 3D Slicer for segmentation practice. In TPS, the head and organs at risk such as the lens and parotid gland, brain, and planning target volume (PTV) were delineated. Gross tumour volume (GTV) and clinical target volume (CTV) were assumed to be within the cranial area with the delineation of PTV involving the whole brain with the entire cranial content. Previous literature reported that a collapsed cone (CC) dose calculation algorithm is based on a separation of primary photon transport and secondary transport of photons and electrons (Victor 2015). The CC dose algorithm decreases the computational time by collapsing the kernels into a certain number of directions (Victor 2015).

An additional margin was imposed in the target region and selected organ of interest to account for patient motion, organ motion and discrepancies in daily positioning during radiotherapy treatment. Additional margin will reduce and minimise the incorrect positioning and direction of the beam to the target region. Contouring the target and organ of interest is often implemented and is a common approach in extracting three dimensional information for treatment planning (Mohan *et al.* 1994).

The variation in the delineation colors represents the target area, OARs and PTV. The delineation closely referred to the treatment planning of an intensity-modulated radiotherapy (IMRT) technique for head and neck cases within the clinical setting. Several organs at risk were delineated, which include eyeballs, lenses, optic nerves, spinal cord, brain stem and parotid glands. For optic nerves and brain stem, a 1.0 mm margin was added to account for uncertainties and labeled as PRV optic nerve and PRV brain stem. For spinal cord, a margin of 5.0 mm was added.

The planning target volume was prioritised in the optimisation process. The dose prescription was set to deliver 3000 cGy in 10 fractions, at 300 cGy per fraction (Arora and Cascella 2021). The dose was prescribed to the isocenter of the beam using a parallel-opposed technique at 6 MV photon energy. The use of parallel fields in WBRT enables coverage of the entire brain (Arora and Cascella 2021). The beam arrangement and weighting were aimed to ensure that at least 95% of the dose would cover the PTV. This arrangement was made after several adjustments to avoid the maximum dose exceeding 107%, adhering to the recommended ICRU Report 50. This percentage was within agreement referring to ICRU Report 50 which recommends target dose uniformity within +7% and -5% (Monti *et al.* 1995). The American Association of Physicists in Medicine report 85 states that a 5% change in dose may result in a significant change in tumour control and normal tissue complication probabilities (Papanikolaou *et al.* 2004). Figure 1 shows the beam eye view (BEV) of the active beam in the plan. Figure 2 shows the 3D view of the parallel-opposed plan. Figure 3 illustrates the fabricated soy-lignin bonded *Rhizophora* spp. head phantom.

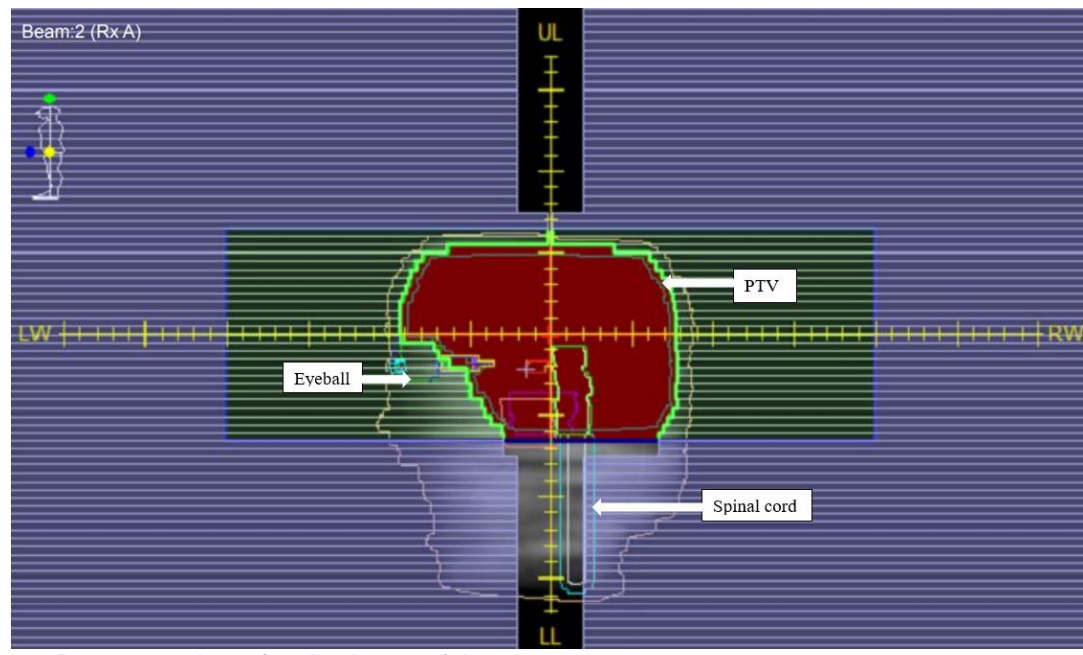
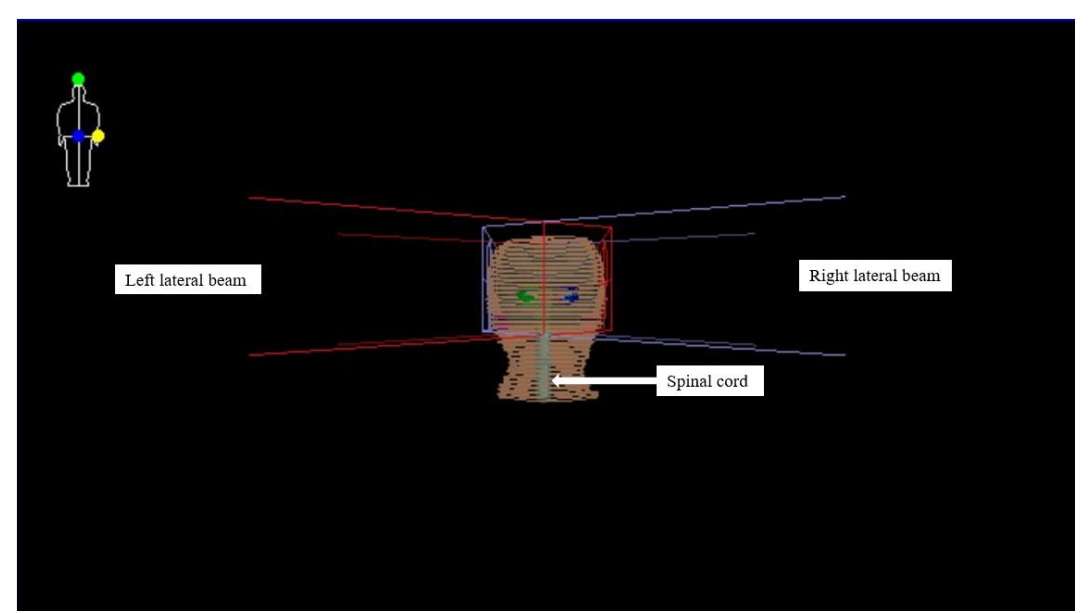


Fig. 1. Beam eye view of active beam of the plan



**Fig. 2.** 3D view of a head phantom during CT simulation in treatment planning software. The phantom is positioned supine, with lateral opposing beams marked in red (left) and blue (right), targeting the central brain volume. Internal structures representing the eyes (green and blue regions) and spinal cord are visualised. The red and blue boxes indicate the beam boundaries, with the isocentre aligned at the mid-brain region.

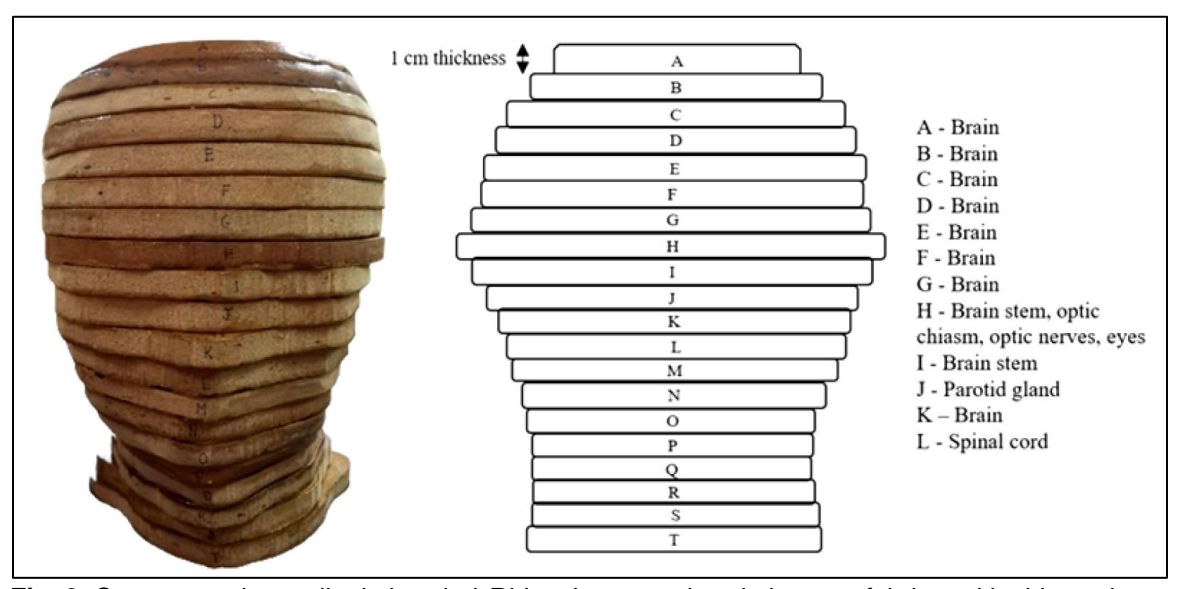


Fig. 3. Custom-made soy-lignin bonded Rhizophora spp. head phantom fabricated in this work

Dose to the organ at risk such as lens, eyeballs, optic nerves, brain stem and spinal cord was taken into consideration during the optimisation procedure to minimise the dose to these structures. However, there was a limitation to maintaining a certain beam arrangement with the fixed organ placement. Hence, the coverage of PTV at least 95 % of the volume achieved was prioritised. Table 1 shows the summary of the beam arrangement used in this study.

 Table 1. Beam Summary Report

| Beam Number               | 1   | 2             |  |
|---------------------------|---|---------------|--|
| Description               | RT Lateral                                | LT Lateral    |  |
| Field ID                  | G270W                                     | G90W          |  |
| Treatment unit            | Synergy                                   | Synergy       |  |
| Machine ID                | SynergyAgility – 6MV SynergyAgility – 6MV |               |  |
| Machine energy            | 6.0 MV 6.0 MV                             |               |  |
| Modality                  | Photon Photon                             |               |  |
| Algorithm                 | Collapsed Cone Collapsed Cone             |               |  |
| Setup                     | SAD                                       | SAD           |  |
| SSD (cm)                  | 92.91                                     | 92.17         |  |
| Gantry (deg)              | 270.0                                     | 90.0          |  |
| Collimator (deg)          | 0.0                                       | 0.0           |  |
| Couch (deg)               | 0.0                                       | 0.0           |  |
| Asymmetric                | Yes                                       | Yes           |  |
| Width 1 (cm)/Label        | 20.00 / LW                                | 20.00 / LW    |  |
| Width 2 (cm)/Label        | 20.00 / RW                                | 20.00 / RW    |  |
| Length 1 (cm)/Label       | 6.50 / UL                                 | 6.50 /UL      |  |
| Length 2 (cm)/Label       | 6.50 / LL                                 | 6.50 / LL     |  |
| MLC model                 | ELEKTAAgility                             | ELEKTAAgility |  |
| Couch                     | Not assigned Not assigned                 |               |  |
| Bolus                     | Not assigned Not assigned                 |               |  |
| Number of blocks          | 0 0                                       |               |  |
| Isocenter x (cm)          | -0.23                                     |               |  |
| Isocenter y (cm)          | 12.89                                     |               |  |
| Isocenter z (cm)          | -1.47                                     |               |  |
| Number of segments        | 0 0                                       |               |  |
| MU/Fx                     | 165.00                                    | 164.88        |  |
| DRP x (cm)                | 0.00                                      | 0.00          |  |
| DRP y (cm)                | 12.45                                     | 12.45         |  |
| DRP z (cm)                | -0.83                                     | -0.83         |  |
| SSD to DRP (cm)           | 92.75                                     | 91.75         |  |
| OAD at isocenter (cm)     | 0.77                                      | 0.78          |  |
| Physical depth (cm)       | 7.48                                      | 8.02          |  |
| Radiological depth (cm)   | 6.71                                      | 7.12          |  |
| Beam dose at DRP/fx (cGy) | 150.0                                     | 150.0         |  |

SSD: source-skin distance; MLC: multi-leaf collimator; MU: Monitor Unit; Fx: fraction; DRP: dose at reference point; OAD: off-axis distance

The point doses were recorded from the selected points on the plan (ROI) in the TPS at about the same points where the TLDs were placed in the phantom. The reading was taken three times and the values were averaged. The quality of the plan was also evaluated based on the dose volume histogram and the data analysis was performed using the heterogeneity index (HI). HI can be defined by various formulas. Over the years, the calculation for HI varies with different indication values that will show if the dose distribution is more homogenous or not (Yan et al. 2019). The ideal formula to calculate HI still remains in discussion and previous literature reported various definitions and formulae, in which none has been described as ideal or near ideal for calculating HI (Thomas and Mathew 2019). HI is known as a simple and fast scoring tool for analysing and quantifying dose homogeneity in the target volume, besides characterising the uniformity of the distribution of the absorbed dose within the target volume (Rodriguez 2018; Yan et al. 2019). It is known that acceptable inhomogeneity was defined as 5% above and 7% below the prescribed dose inside the target volumes. An inhomogeneity coefficient (IC) of the dose in the target volumes were calculated using the formula in Equation 1 (Harrabi et al. 2016).

$$IC = \frac{D_{max} - D_{min}}{D_{mean}} \tag{1}$$

where  $D_{max}$  and  $D_{min}$  are the maximum and minimum doses in the PTV, respectively, and  $D_{mean}$  is the average PTV dose. Previous literature reported that the closer the IC to zero, the more homogenous the plan was considered (Zach *et al.* 2009).

## Irradiation of Head Phantom at 6 MV Photon Energy to Calculate for TLD Absorbed Dose

The linearity, reproducibility, and calibration procedures for the thermoluminescent dosimeter (TLD-100H) were thoroughly investigated in a previous study by Binti Zuber et al. (2023) as part of the groundwork for the current research. That study established the TLDs' performance characteristics under controlled conditions, including the development of a reliable calibration curve and evaluation of measurement linearity and reproducibility. These validated procedures formed the basis for the dosimetric measurements carried out in this work, ensuring accuracy and reliability in the absorbed dose assessment (binti Zuber et al. 2023).

The TLDs were placed in their designated locations on the custom-made head phantom in order to assess point dose. The phantom contains a number of TLD holes strategically placed at different target areas. To allow for dose assessment in the designated positions, the holes were labeled. Several depths of the phantom were used to measure the dose, which would not have been achievable using in-vivo dosimetry (Abdemanafi *et al.* 2020). The phantom was irradiated by 6 MV photon energy with the dose of 300 cGy in one fraction, using the linear accelerator Elekta Synergy Agility LINAC (Elekta Medical Systems, Crawley, UK) with Precise Multi-leaf Collimators (MLCs), employing the lateral opposed fields designed at 90° and 270° gantry angles. The readings were repeated three times and the results were averaged. Finally, measurements of the TLD absorbed dose were compared to the TPS Monaco dose estimations produced from the DVH.

#### **TLD Dose Measurement**

TLDs (TLD-100H, LiF:Mg,Cu,P) in chip form with the dimension of  $(3.2 \times 3.2 \times$ 0.38) mm<sup>3</sup>, with a linear energy range of 1 µGy to 10 Gy, were provided by Thermo Fisher Scientific (Harshaw Company, Kuala Lumpur, Malaysia) and were subjected to linearity, reproducibility and calibration tests prior to the dose measurement. The finding reveals the linear relationship between the dose given and the charges collected based on each TLD's dose-response curves. Individual calibration was performed for every TLD and the calibration curves were employed for the dose calculation in this study. Before irradiation, TLDs were annealed at the temperature of 200 °C for 1 hour and 10 minutes followed by 50 °C for 30 minutes using the TLD furnace. For this study, the TLDs were placed in predetermined positions within the phantom slabs representing different target areas and organs, and the phantom was irradiated at 6 MV photon energy with the prescribed dose of 3000 cGy in 10 fractions. TLDs were kept in a room condition for approximately 24 hours post-irradiation before they were read. Pre-set Time Temperature Profile Setup (TTP) was used in this study with a temperature rate of 10 °C/s with a maximum temperature of 300 °C. Each measurement point yielded three readings and Thermo-Scientific Model 3500, a manually controlled TLD Reader system, was used to manually

read the TLDs which were averaged to obtain the TLD measured dose for that measurement location.

#### **RESULTS AND DISCUSSION**

### HI, IC Values and Dose Comparison Between TLD and TPS

The analysis of HI was performed during the treatment planning process and the results revealed a HI value of 1.06. Previous literature reported that the IC evaluates the distribution variance of the dose in PTV, where higher values show greater variability (Claus *et al.* 2002). The calculated IC value of PTV is 0.364, which is close to zero, which may indicate a homogenous plan.

The TLDs positioned in each slab were irradiated following the treatment planning using the 6 MV photon. In this study, the measured dose using TLDs and the estimation of dose by TPS were quantified. This treatment planning generated 98.68 % of the target dose covering 95 % of PTV with maximum a dose of 106.8 %. In this planning, total PTV coverage was difficult due to the large PTV area comprising the whole brain, and to avoid hotspots exceeding 107 %. The dose constraint value was provided by previous literature (Lee *et al.* 2006; Emami 2013; Radaideh *et al.* 2013; Basu and Bhaskar 2018). Table 2 illustrates the measured dose by TLDs and dose estimation by TPS.

Table 2. Summary of measured doses by TLDs and TPS

| Structures          | Dose Constraint<br>(Gy) | Average Dose<br>Reading by TLD<br>(cGy) | Range of Absorbed Dose by<br>TPS (cGy) |
|---------------------|-------------------------|---|--|
| PTV                 | <65 <sup>a</sup>        | 227.43                                  | 209.41-320.36                          |
| Spinal cord         | <45                     | 178.87                                  | 2.16–225.94                            |
| Right parotid gland | <26                     | 183.96                                  | 144.66–307.19                          |
| Left parotid gland  | <26                     | 206.47                                  | 134.25–307.04                          |
| Brainstem           | <54                     | 211.31                                  | 243.82-307.53                          |
| Optic chiasm        | <54                     | 185.36                                  | 293.36-298.75                          |
| Right optic nerve   | <55 <sup>a</sup>        | 191.84                                  | 56.24-300.10                           |
| Left optic nerve    | <55 <sup>a</sup>        | 197.67                                  | 55.77-299.89                           |
| Right eye           | <45                     | 53.44                                   | 13.85–237.24                           |
| Left eye            | <45                     | 55.43                                   | 12.50–245.47                           |
| Left lens           | 5-10 <sup>b</sup>       | 55.41                                   | 18.23-44.36                            |

PTV: planning target volume

(Emami 2013)a; (Basu and Bhaskar 2018)b

Based on the result, the average TLD dose recorded in PTV is 227.43 cGy, which is within the range of absorbed dose by TPS, however quite low as compared to the prescribed dose. This may be attributed to repetitive TLD reading, annealing and transferring process which may degrade its ability to better store the charge. According to a study by the International Atomic Energy Agency (IAEA), there is a 5.8% TLD uncertainty for megavoltage photon beams due to repetitive TLD measurement uncertainties, absorbed dose energy dependence, energy-dependence corrections, uncertainties in LINAC and TLD calibration and uncertainties in TLD positioning (Absorbed Dose Determination in External Beam Radiotherapy 2001; Castro et al. 2008). Another study revealed an estimation of 5% TLD readout uncertainty by considering several factors which include repetitive TLD measurements, calibration and positioning uncertainty, besides the energy dependence correction (Almond et al. 1999). Other than

that, the previous study also suggested a 5% acceptable difference between the TPS and TLD dose measurements for external photon beams (Van Dyk *et al.* 1993). Previous literature reported that certain radiotherapy centres pre-set the acceptance criteria as 5 % at high-dose regions (PTV) and 10 % at low-dose regions (OAR) for dose verification in a phantom with TLD, MOSFET and ion chambers (Radaideh *et al.* 2013).

The PTV and OARs were within the dose ranges calculated by TPS, except for the lens, optic chiasm and brainstem. Such disparity may be due to the position of each slab that may slightly change and the misalignment of TLD as the procedure was repeated several times. Lower dose measured in brainstem may be due to the scratching and breaking of TLDs which cannot be avoided due to their repetitive usage in the dose measurement procedure, thus reducing the light emission for a given radiation exposure (Darafsheh, 2021). Other than that, such discrepancy in the absorbed dose may be attributed to the air gaps within the TLD holes (Radaideh 2017). It is also worth noting that the coefficient of variation value of the TLD representing the optic chiasm is higher than 7.5% but below 10% (IEC 62387 2012; Sadeghi *et al.* 2015), which may also affect the overall TLD reading.

For the lens, TLDs representing the lens were placed near the surface of the phantom, which may result in over- or under-estimation of dose due to the algorithm limitation at the material interface (Dobler *et al.* 2006). Over or under-estimation of the dose in the lens can also be caused by the dose in the lens being measured inside the eyes, whereas, while measuring with the TLD, it is placed on the surface, which refers to the entrance dose of an eye. Previous literature also reported that TPS overestimated the surface dose for both shallow and deep target cases, with the amount of over-estimation ranging from 400 to 1000 cGy (Chung *et al.* 2005). The sparing of the OARs, given their various size within or at a distance from the PTV, may depend on the MLC leaf width and the reported doses may also be significantly influenced by the penumbra widths relating to how these were modeled in the TPS.

A higher absorbed dose measured by TPS can be observed in this study. Small positional errors in the TLD measurements may be the cause of this effect rather than TPS inaccuracy near the target volume. TLD positioning errors in the phantom may be contributed by inaccurate placement within the designated holes, slight tilting or shifting during setup, variations in depth insertion, or inconsistencies in hole alignment during the fabrication process. Other than that, the small size of the TLDs may significantly influence the comparative study of the planned and measured doses as it may not be accurately traced in the TPS for the dose calculation. Incorrect tracing of the TLDs may also result in inaccurate dot dosing optimisation in the TLD (Kowalik *et al.* 2019). Previous literature reported that it may not be possible to precisely contour objects of such small dimensions using the current contouring system (Kowalik *et al.* 2019).

The dose disparity between the TPS and TLD may also be due to the limitations of the TPS dose calculation algorithm in homogeneous regions, inaccurate beam modelling and inherent limitations of the TLDs. Material inhomogeneity can also affect the dose measured in the phantom by altering the attenuation and scattering properties of the material. Variations in density, composition, or structural consistency such as air gaps, uneven bonding, or inconsistent particle packing can cause local under- or over-response in dose measurements, thus introducing discrepancies between the TLD-measured dose and the TPS-calculated dose. The higher absorbed dose recorded by TPS may also be due to inaccurate modelling of the dose contributions from contaminated electrons and secondary scatter photons derived from the accelerator head. Previous literature reported

that one of the key sources of errors in TPS is the dose computation of each spot to obtain the truly optimum final dose distribution. Inaccuracies in the spot dose distributions inevitably lead to systematic errors in the spot weights and may even be amplified in the optimisation (Jeraj *et al.* 2002).

The absorbed doses to PTV and OARs using TLD were within their respective tolerance dose levels except for the lens, which may be attributed to its location within the phantom. Better protection of the OARs will thereby lower the normal tissue complication probabilities (Grzadziel *et al.* 2006). Two separate courses of radiotherapy may be required although the risk of the field overlap that may cause hot spots and some inhomogeneity in dose distributions have to be considered. It is known that accurate head dose assessment is particularly challenging because of the complexity of the structure itself. Further analysis of treatment planning is advised since it may be necessary to conduct ongoing quality assurance tests due to the depth and complexity of the treatment planning.

The findings on the custom-made, bio-based Rhizophora phantom have demonstrated its significant value as a tool for verifying treatment doses in radiotherapy. This innovative bio-based phantom, represents a key step forward in merging sustainability with clinical performance. Its composition, made from soy-lignin bonded *Rhizophora* spp., mimics the physical and radiological properties of human tissue, offering reliable attenuation and interaction characteristics. Clinically, this bio-based phantom provides several practical advantages. Its anatomical customisability and compatibility with TLD measurements make it a suitable model for accurate dose verification, treatment planning validation, and radiotherapy quality assurance. Moreover, its cost-effectiveness and mechanical durability position it as a feasible alternative to expensive commercial phantoms, facilitating broader accessibility in both training and clinical practice. Environmentally, the use of locally sourced, biodegradable materials supports global efforts toward reducing the ecological footprint of healthcare technologies. By integrating eco-conscious material design into radiotherapy tools, this phantom reflects a growing commitment to green innovation in medical physics. Overall, the study demonstrated the phantom's potential not only as a reliable dosimetric tool but also as a sustainable, clinically relevant solution that aligns with modern environmental and healthcare priorities.

#### CONCLUSIONS

In this study, a bio-based head phantom made from soy-lignin-bonded *Rhizophora* spp. was fabricated. Organs at risk and planning target volume were identified using the treatment planning system, which was guided by computed tomography raw images.

- 1. Good agreement of absorbed dose received by target of interest and organs at risk between measured values by TLD and those predicted by TPS was found.
- 2. The PTV and OARs were within the dose range calculated by TPS, except for lens, optic chiasm and brainstem.
- 3. The findings reveal that the bio-based head phantom, made from renewable natural resources, has potential as a dosimetric phantom in radiotherapy, particularly for treatment planning.

#### **ACKNOWLEDGMENTS**

The authors acknowledge the Universiti Kebangsaan Malaysia Geran Galakan Penyelidik Muda (GGPM-2023-027), Universiti Sains Malaysia Short-Term Grant (304/PFIZIK/6315322) and the Universiti Sains Malaysia Bridging Grant (304.PPSK.6316324).

#### REFERENCES CITED

- Abdemanafi, M., Tavakoli, M. B., Akhavan, A., and Abedi, I. (2020). "Evaluation of the lung dose in three-dimensional conformal radiation therapy of left-sided breast cancer: A phantom study," *J. Med. Signals Sens.* 10, 48–52. DOI: 10.4103/jmss.JMSS\_1\_19
- Almond, P. R., Biggs, P. J., Coursey, B. M., Hanson, W.F., Huq, M.S., Nath, R., and Rogers, D.W. (1999). "AAPM's TG-51 protocol for clinical reference dosimetry of high-energy photon and electron beams," *Med. Phys.* 26, 1847–1870. DOI:10.1118/1.598691
- Armocida, D., Pesce, A., Palmieri, M., Cofano, F., Palmieri, G., Cassoni, P., Busceti, C.L., Biagioni, F., Garbossa, D., Fornai, F., *et al.* (2023). "EGFR-driven mutation in non-small-cell lung cancer (NSCLC) influences the features and outcome of brain metastases," *J. Clin. Med.* 12(10), 3372. DOI:10.3390/jcm12103372
- Arora, R. D., and Cascella, M. (2021). *Palliative Radiation Therapy for Brain Metastases*, Treasure Island (FL).
- Basu, T., and Bhaskar, N. (2018). "Overview of important "organs at risk" (OAR) in modern radiotherapy for head and neck cancer (HNC)," in: *Cancer Survivorship* DOI:10.5772/intechopen.80606
- binti Zuber, S. H., Hadi, M.F.R.A., Hashikin, N.A.A., Yusof, M.F.M., and Aziz, M.Z.A. (2024). "Rhizophora-based particleboard bonded with soy flour and lignin as potential phantom," *BioResources* 19(3), 5467–5482. DOI: 10.15376/biores.19.3.5467-5482
- Castro, P., García-Vicente, F., Mínguez, C., Floriano, A., Sevillano, D., Pérez, L., and Torres, J. J. (2008). "Study of the uncertainty in the determination of the absorbed dose to water during external beam radiotherapy calibration," *J. Appl. Clin. Med. Phys.* 9, 70–86. DOI: 10.1120/jacmp.v9i1.2676
- Cederhag, J., Kadesjö, N., Nilsson, M., Alstergren, P., Shi, X.-Q., and Hellén-Halme, K. (2023). "Comparison of absorbed doses and organ doses measured with thermoluminescent dosimeters and Gafchromic film for cone beam computed tomography examination of the posterior mandibular region in a head phantom," *Oral Surg. Oral Med. Oral Pathol. Oral Radiol.* 136(6), 769-776. DOI:10.1016/j.0000.2023.07.006
- Chavaudra, J., and Bridier, A. (2001). "Définition des volumes en radiothérapie externe : rapports ICRU 50 et 62," *Cancer/Radiothérapie* 5, 472–478. DOI:10.1016/S1278-3218(01)00117-2
- Chung, H., Jin, H., Dempsey, J. F., Liu, C., Palta, J., Suh, T.-S., and Kim, S. (2005). "Evaluation of surface and build-up region dose for intensity-modulated radiation therapy in head and neck cancer," *Med. Phys.* 32, 2682–2689. DOI:10.1118/1.1992067

- Claus, F., Mijnheer, B., Rasch, C., Bortfeld, T., Fraass, B., De Gersem, W., Wirtz, H., Hoinkis, C., Cho, B.C., Kwong, L.W.D., *et al.* (2002). "Report of a study on IMRT planning strategies for ethmoid sinus cancer," *Strahlenther. Onkol.* 178, 572–576. DOI:10.1007/s00066-002-0999-3
- Darafsheh, A. (2021). "Radiation therapy dosimetry: A practical handbook," *CRC Press*.
  Dobler, B., Walter, C., Knopf, A., Fabri, D., Loeschel, R., Polednik, M., Schneider, F., Wenz, F., and Lohr, F. (2006). "Optimization of extracranial stereotactic radiation therapy of small lung lesions using accurate dose calculation algorithms," *Radiat*. *Oncol.* 1, 45. DOI:10.1186/1748-717X-1-45
- Emami, B. (2013). "Tolerance of normal tissue to therapeutic radiation," *Reports Radiother. Oncol.* 1.
- Gao, Y., Gao, F., Ma, J.-L., and Zhao, D.-L. (2015). "Palliative whole-brain radiotherapy and health- related quality of life for patients with brain metastasis in cancer," *Neuropsychiatr. Dis. Treat.* 11, 2185–2190. DOI:10.2147/NDT.S87109
- Gibbs, I. C., and Soltys, S.G. (2008). "Central nervous system metastases," in: J.J. Lu, L. W. Brady (eds.) *Radiation Oncology. Medical Radiology*. Springer, Berlin, Heidelberg. DOI: 10.1007/978-3-540-77385-6\_44
- Grzadziel, A., Grosu, A.-L., and Kneschaurek, P. (2006). "Three-dimensional conformal versus intensity-modulated radiotherapy dose planning in stereotactic radiotherapy: Application of standard quality parameters for plan evaluation," *Int. J. Radiat. Oncol. Biol. Phys.* 66, S87–S94. DOI:10.1016/j.ijrobp.2006.01.056
- Gupta, T., Basu, A., Master, Z., Jalali, R., Munshi, A., and Sarin, R. (2009). "Planning and delivery of whole brain radiation therapy with simultaneous integrated boost to brain metastases and synchronous limited-field thoracic radiotherapy using helical tomotherapy: A preliminary experience," *Technol. Cancer Res. Treat.* 8, 15–22. DOI:10.1177/153303460900800103
- Hamilton, S. E., and Casey, D. (2016). "Creation of a high spatio-temporal resolution global database of continuous mangrove forest cover for the 21st century (CGMFC-21)," *Glob. Ecol. Biogeogr.* 25, 729–738. DOI:10.1111/geb.12449
- Harrabi, S. B., Bougatf, N., Mohr, A., Haberer, T., Herfarth, K., Combs, S.E., Debus, J., and Adeberg, S. (2016). "Dosimetric advantages of proton therapy over conventional radiotherapy with photons in young patients and adults with low-grade glioma," *Strahlenther. Onkol.* 192, 759–769. DOI:10.1007/s00066-016-1005-9
- IEC 62387 (2012). "Radiation protection instrumentation—passive integrating dosimetry systems for personal and environmental monitoring of photon and beta radiation," International Electrotechnical Commission.
- IAEA (2001). "Absorbed dose determination in external beam radiotherapy," Technical Reports Series, International Atomic Energy Agency, Vienna.
- Jeraj, R., Keall, P., and Siebers, J. (2002). "The effect of dose calculation accuracy on inverse treatment planning," *Phys. Med. Biol.* 47, 391–407. DOI:0.1088/0031-9155/47/3/303
- Kowalik, A., Konstanty, E., Piotrowski, T., Skórska, M., and Malicki, J. (2019). "Calculation and measurement of doses in the surface layers of a phantom when using Tomotherapy," *Reports Pract. Oncol. Radiother.* 24, 251–262. DOI:10.1016/j.rpor.2018.11.006
- Lee, N., Pfister, D. G., and Garden, A. (2006). "A phase II study of concurrent chemoradiotherapy using 3-D conformal radiotherapy (3D-CRT) or intensity-modulated radiation therapy (IMRT) + bevacizumab (BV) for locally or regionally

- advanced nasopharyngeal cancer," RTOG-0615 Protocol
- Mohan, R., Wang, X., Jackson, A., Bortfeld, T., Boyer, A. L., Kutcher, G. J., Leibel, S. A., Fuks, Z., and Clifton Ling, C. (1994). "The potential and limitations of the inverse radiotherapy technique," *Radiother. Oncol.* 32, 232–248. DOI:10.1016/0167-8140(94)90023-X
- Monti, A. F., Ostinelli, A., Frigerio, M., Cosentino, D., Bossi, A., Cazzaniga, L.F., Scandolaro, L., and Valli, M. C. (1995). "An ICRU 50 radiotherapy treatment chart," *Radiother. Oncol.* 35, 145–150. DOI:10.1016/0167-8140(95)01541-N
- Papanikolaou, N., Battista, J., Boyer, A., Kappas, C., Klein, E., Mackie, T., Sharpe, M., and Van Dyk, J. (2004). "Tissue inhomogeneity corrections for megavoltage photon beams," AAPM Report No. 85, Task Group No 65 of the Radiation Therapy Committee of the American Association of Physicists in Medicine.
- Park, J., Park, J. W., and Yea, J. W. (2019). "Non-coplanar whole brain radiotherapy is an effective modality for parotid sparing," *Yeungnam Univ. J. Med.* 36, 36–42. DOI:10.12701/yujm.2019.00087
- Radaideh, K. M. (2017). "A custom made phantom for dosimetric audit and quality assurance of three-dimensional conformal radiotherapy," *J. Sains Nukl. Malaysia* 24, 48–58.
- Radaideh, K. M., Matalqah, L.M., Tajuddin, A. A., Lee, W. I. F., Bauk, S., and Eid Abdel Munem, E. M. (2013). "Development and evaluation of a Perspex anthropomorphic head and neck phantom for three dimensional conformal radiation therapy (3D-CRT)," *J. Radiother. Pract.* 12, 272–280. DOI:10.1017/S1460396912000453
- Rodriguez, W. (2018). "Comparison between 3D-CRT and modulated techniques for head-and-neck and breast," *AIP Conference Proceedings*. DOI:10.1063/1.5050360
- Sadeghi, M., Sina, S., and Faghihi, R. (2015). "Investigation of Lif, mg and Ti (TLD-100) reproducibility," *J. Biomed. Phys. Eng.* 5, 217.
- Thomas, F. K. S., and Mathew, M. P, K. (2019). "Impact of homogeneity index on response rate and survival in head and neck cancer patients treated with IMRT," *J. Evol. Med. Dent. Sci.* 8, 62–66. DOI:10.14260/jemds/2019/14
- Tootell, A., Szczepura, K., and Hogg, P. (2014). "An overview of measuring and modelling dose and risk from ionising radiation for medical exposures," *Radiography* 20, 323–332. DOI:10.1016/j.radi.2014.05.002
- Van Dyk, J., Barnett, R. B., Cygler, J. E., and Shragge, P. C. (1993). "Commissioning and quality assurance of treatment planning computers," *Int. J. Radiat. Oncol. Biol. Phys.* 26, 261–273. DOI:10.1016/0360-3016(93)90206-b
- VanDam, J., and Marinello, G. (1994). "Methods for *in vivo* dosimetry in external radiotherapy," *Garant Publ*.
- Victor, L. (2015). "The difference between a collapsed cone based and a Monte Carlo based dose calculation algorithm," RaySearch Lab. Stock, Sweden.
- Vlachos, N., Lampros, M.G., Filis, P., Voulgaris, S., and Alexiou, G.A. (2023). "Stereotactic radiosurgery versus whole-brain radiotherapy after resection of solitary brain metastasis: A systematic review and meta-analysis," *World Neurosurg. X* 18, 100170. DOI:10.1016/j.wnsx.2023.100170
- Wesolowska, P.E., Cole, A., Santos, T., Bokulic, T., Kazantsev, P., Izewska, J. (2017). "Characterization of three solid state dosimetry systems for use in high energy photon dosimetry audits in radiotherapy," *Radiat. Meas.* 106, 556–562. DOI:10.1016/j.radmeas.2017.04.017

- Yadav, N., Singh, M., Mishra, S.P., Ansari, S. (2023). "Development of an anthropomorphic heterogeneous female pelvic phantom and its comparison with a homogeneous phantom in advance radiation therapy: Dosimetry analysis," *Med. Sci.* 11(3), 59. DOI:10.3390/medsci11030059
- Yan, L., Xu, Y., Chen, X., Xie, X., Liang, B., and Dai, J. (2019). "A new homogeneity index definition for evaluation of radiotherapy plans," *J. Appl. Clin. Med. Phys.* 20, 50–56. DOI:10.1002/acm2.12739
- Zach, L., Stall, B., Ning, H., Ondos, J., Arora, B., Uma, S., Miller, R.W., Citrin, D., and Camphausen, K. (2009). "A dosimetric comparison of four treatment planning methods for high grade glioma," *Radiat. Oncol.* 4, 45. DOI:10.1186/1748-717X-4-45
- Zuber, S. H., Hashikin, N.A.A., Mohd Yusof, M.F., and Hashim, R. (2020a). "Physical and mechanical properties of soy-lignin bonded rhizophora spp. particleboard as a tissue-equivalent phantom material," *BioResources* 15(3), 5558-5576. DOI: 10.15376/biores.15.3.5558-5576
- Zuber, S. H., Hashikin, N. A. A., Mohd Yusof, M. F., and Hashim, R. (2020b). "Investigation on Suitable coating material for soy-lignin bonded rhizophora spp. particleboard for medical physics applications," *BioResources* 15(4), 7404-7419. DOI: 10.15376/biores.15.4.7404-7419
- Zuber, S. H., Abdul Hadi, M. F. R., Hashikin, N. A. A., Yusof, M. F. M., Aziz, M. Z. A., Hashim, R., Oluwafemi, S. D., and Isa, N. M. (2022a). "Estimation of linear and mass attenuation coefficients of soy–lignin bonded Rhizophora spp. particleboard as a potential phantom material using caesium-137 and cobalt-60," *Radiat. Environ. Biophys.* 61, 435–443. DOI:10.1007/s00411-022-00978-2
- Zuber, S. H., Hadi, M.F.R.A., Oluwafemi, S.D., and Fahmi, M. (2022b). "Compton Scrattering study using ludlum configuration for tissue-equivalent phantom material made from soy-lignin bonded Rhizophora spp. particleboard," *Sains Malaysiana* 51, 1895–1904. DOI:10.17576/jsm-2022-5106-24
- Zuber, S. H., Hashikin, N. A. A., Mohd Yusof, M. F., Aziz, M. Z. A., and Hashim, R. (2021). "Characterization of soy-lignin bonded Rhizophora spp. particleboard as substitute phantom material for radiation dosimetric studies Investigation of CT number, mass attenuation coefficient and effective atomic number," *Appl. Radiat. Isot. Incl. data, Instrum. methods use Agric. Ind. Med.* 170, 109601. DOI:10.1016/j.apradiso.2021.109601

Article submitted: November 21, 2024; Peer review completed: March 7, 2025; Revisions accepted: May 20, 2025; Published: May 23, 2025.

DOI: 10.15376/biores.20.3.5694-5708